Supplemental figures

Figure S1.

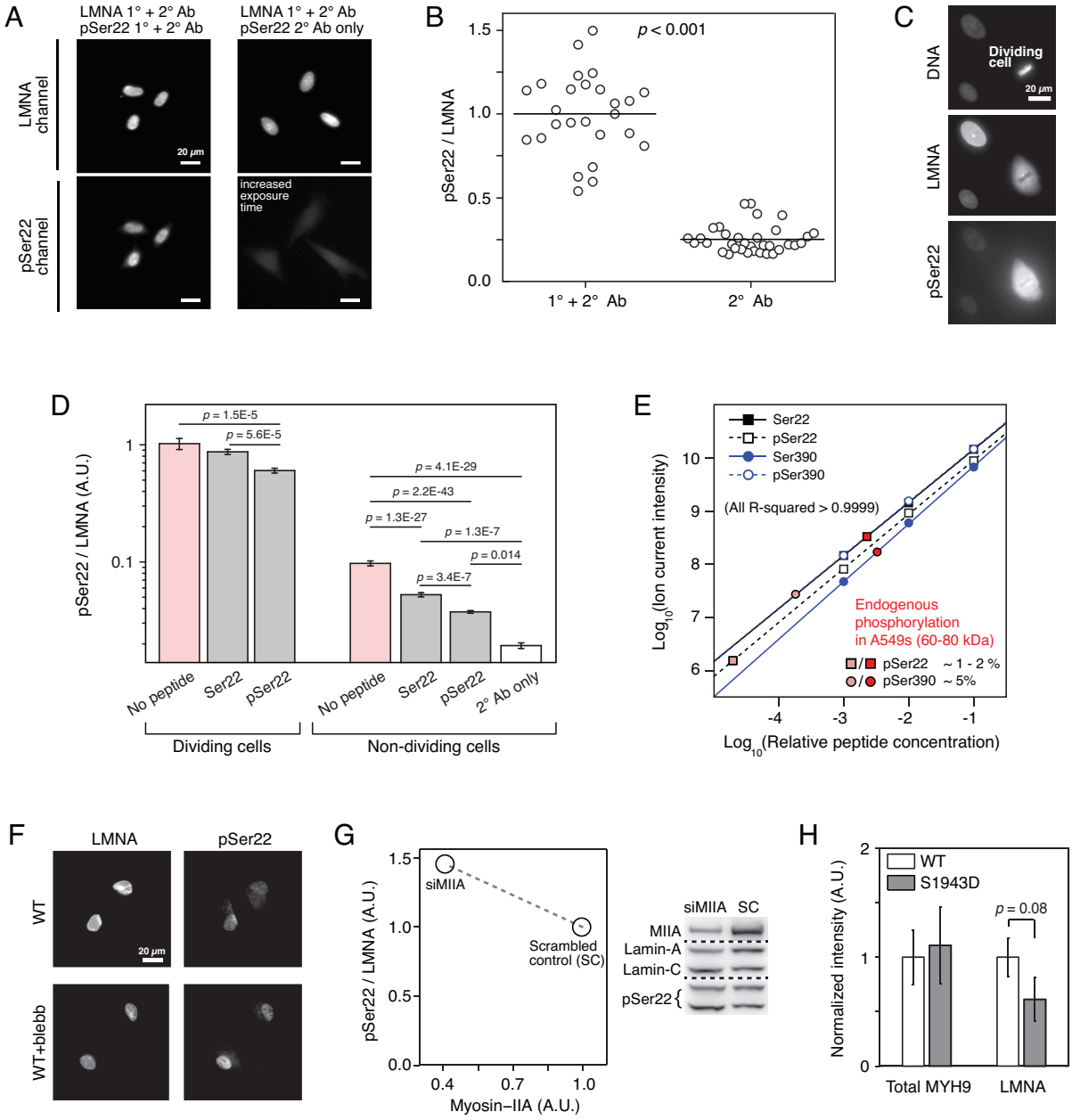

Figure S1.

(Related to Figs. 1A, B) pSer22 immunostain of all interphase nuclei is > 2° antibody (Ab) control, but << dividing cells. (**A**) Immunostaining specificity to the pSer22 epitope was demonstrated in A549 cells by comparison to secondary antibody-only staining, in conjunction with staining for lamin-A,C (LMNA) that was imaged in a different channel. Note that the exposure time is increased in the bottom-right panel to show that non-specific binding is not localized to the nucleus. (**B**) Antibody binding to pSer22 was found to be four-fold higher than secondary-only non-specific binding. (**C**) Antibody specificity to the phosphorylated epitope was confirmed by a higher pSer22 immunostaining intensity in cells undergoing mitosis.

(Related to Fig. 1B) Calibration of endogenous pSer22 using immunostaining and calibrated mass spectrometry. (**D**) Plot showing normalized pSer22/LMNA intensity ratio in dividing and non-dividing A549 cells, with addition of phosphorylated and non-phosphorylated Ser22 peptides, and a secondary-antibody only control. The Ser22 peptide showed some non-specific blocking of the pSer22 antibody, but was always significantly distinguishable from when blocking with the pSer22 peptide. (**E**) To evaluate pSer22/LMNA stoichiometry in interphase cells, full length (i.e. not proteolytically degraded) lamin-A,C from an A549 cell lysate was obtained from the 60-80 kDa region of an SDS-PAGE gel and interrogated by MS. The extent of phosphorylation was calibrated relative to synthetic peptides: 1-2% of lamin-A,C was found to be phosphorylated at Ser22. A similar treatment showed ~ 5% of lamin-A,C to be phosphorylated at Ser390. Immunoblotting densitometry of the entire SDS-PAGE gel lane (i.e. inclusive of proteolytic lamin fragments) showed that ~ 20% of total pSer22 was from intact, non-degraded lamin-A,C in MSCs (Figs. 3A, B; S3A, B). Assuming pSer22 stoichiometry of intact lamin-A,C to be 1-2% in MSCs, the fraction of pSer22 epitopes relative to total lamin-A,C would be 5-10%. Dividing cells (< 1% of the population) showed 10-fold higher pSer22 intensity than interphase cells (Fig. 1B), suggesting that 50-100% of lamin-A,C was phosphorylated during mitotic breakdown of the nuclear envelope (consistent with Fig. S1C).

(Related to Fig. 1E) Effect of myosin-IIA on lamin-A,C regulation. (**F**) Representative images of MSCs at 2 hours of adhesion, with and without blebbistatin (blebb) treatment. LMNA levels were lower in

blebb treated cells, but the level of pSer22 relative to LMNA was high (quantitative image analysis is shown in Fig. 1E). (**G**) siRNA knockdown of myosin-IIA lead to a lower fraction of LMNA being phosphorylated at Ser22, as determined by quantitative immunoblotting. (**H**) In MSCs expressing a phosphomimetic S1943D mutant GFP-myosin-IIA construct, which suppresses stress-fiber formation [S1, S2], total myosin-IIA levels are the same as those in cells expressing a WT construct, but lamin-A,C is down-regulated consistent with a low contractility phenotype ($n > 90$ cells per group; bars show ± SEM).

Figure S2.

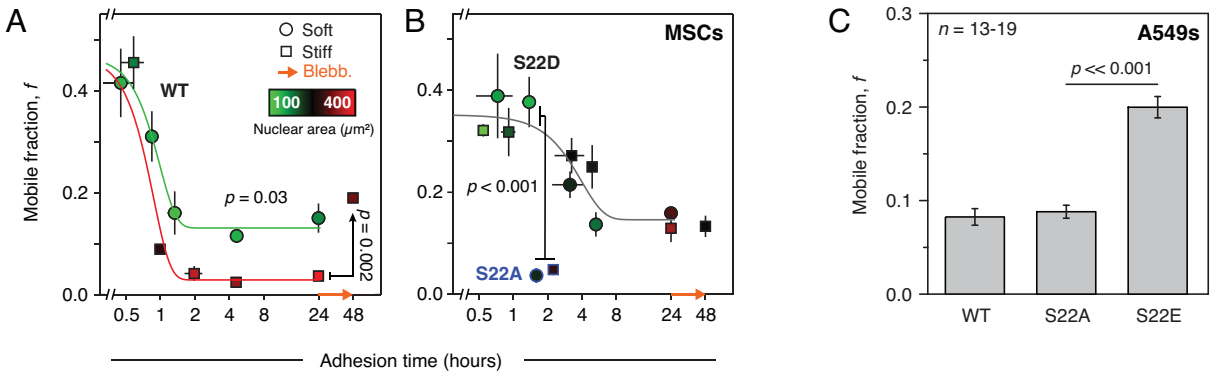

Figure S2.

(Related to Fig. 2) **Mobile GFP-lamin-A fraction in MSCs (as a function of adhesion time) and A549s.** The mobile fraction of a GFP-lamin-A construct, *f*, was evaluated by fitting an exponential curve to the intensity recovery following photobleaching (Fig. 2A). (**A**) f_{WT} decreased with adhesion time of MSCs for the first 2 hours, reaching ~15% on soft (0.3 kPa) but less than 5% on stiff gels (40 kPa) (3-5 nuclei grouped per time point; projected nuclear areas are indicated by the color of each point). Lamin-A mobility was increased by blebb treatment after 24 hours on stiff gels. (**B**) Independent of matrix stiffness, S22D mobile fractions decayed three folds slower than WT, whereas S22A remained immobile. Soft matrices and blebb drive WT lamin-A solubilization, but S22D and S22A show no matrix or blebb dependence (summarized in Fig. 2B). (**C**) Consistent with observations in MSCs, fluorescence recovery experiments using A549 cells showed a greater mobile fraction with phosphomimetic GFP-lamin-A S22E than with WT or non-phosphorylatable S22A.

Figure S3.

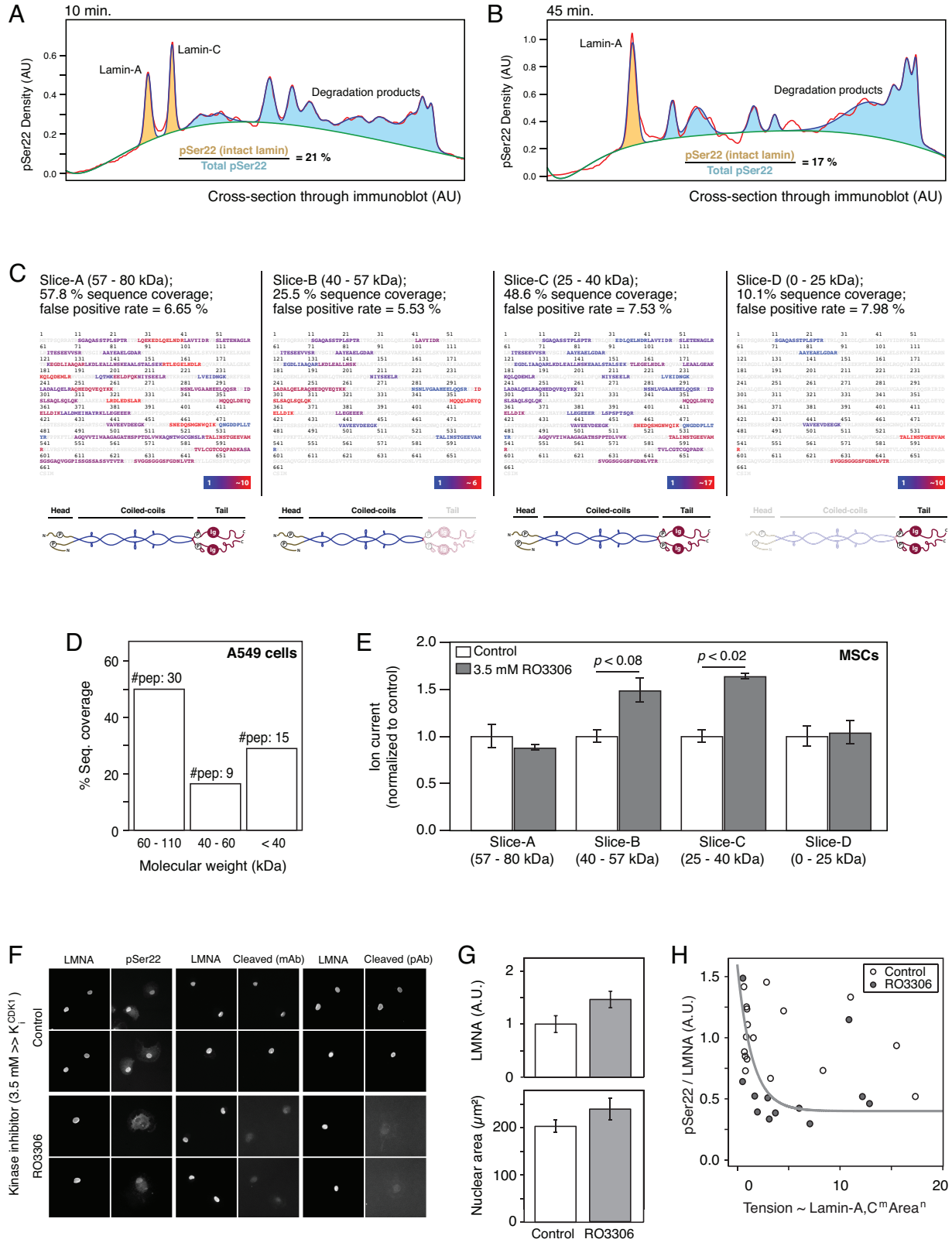
A
10 min.
Lamin-A
Lamin-C
Degradation products
pSer22 (intact lamin)
Total pSer22
= 21 %
pSer22 Density (AU)
Cross-section through immunoblot (AU)
B
45 min.
Lamin-A
Degradation products
pSer22 (intact lamin)
Total pSer22
= 17 %
pSer22 Density (AU)
Cross-section through immunoblot (AU)
C
Slice-A (57 - 80 kDa);
57.8 % sequence coverage;
false positive rate = 6.65 %
Slice-B (40 - 57 kDa);
25.5 % sequence coverage;
false positive rate = 5.53 %
Slice-C (25 - 40 kDa);
48.6 % sequence coverage;
false positive rate = 7.53 %
Slice-D (0 - 25 kDa);
10.1% sequence coverage;
false positive rate = 7.98 %
Head
Coiled-coils
Tail
D
A549 cells
#pep: 30
#pep: 9
#pep: 15
% Seq. coverage
60 - 110
40 - 60
< 40
Molecular weight (kDa)
E
Control
3.5 mM RO3306
p < 0.08
p < 0.02
MSCs
Ion current
(normalized to control)
Slice-A
(57 - 80 kDa)
Slice-B
(40 - 57 kDa)
Slice-C
(25 - 40 kDa)
Slice-D
(0 - 25 kDa)
F
LMNA
pSer22
LMNA
Cleaved (mAb)
LMNA
Cleaved (pAb)
Kinase inhibitor (3.5 mM >> K$_i^{CDK1}$)
Control
RO3306
G
LMNA (A.U.)
Nuclear area (μm²)
Control
RO3306
H
Control
RO3306
pSer22 / LMNA (A.U.)
Tension ~ Lamin-A,C^{m}Area^n

Figure S3.

(Related to Figs. 3A, B) Densitometry of lamin pSer22 western blots. (**A**, **B**) Mesenchymal stem cells (MSCs) were lysed following 10 or 45 minutes in suspension and analyzed by immunoblotting against lamin-A,C and pSer22 (Fig. 3A). Densitometry analysis showed that the majority of the phosphorylated lamin-A,C was fragmented below the expected molecular weight (MW; 75 kDa for lamin-A; 65 kDa for lamin-C).

(Related to Figs. 3C, D) Sequence coverage of lamin-A,C fragments. (**C**) The MSC lysate was separated by SDS-PAGE and analyzed in discrete MW ranges by MS (Fig. 3B), confirming that lamin fragments were found at lower MW. While peptide coverage clearly extended across all weight ranges, slice-D (< 25 kDa) showed an enrichment of tail-domain and Ig-fold peptides whereas slice-B (40-57 kDa) showed head and coiled-coil rod domains. Relative coverage intensity (i.e. signal strength of tryptic peptides) is indicated by the color of the sequence. Sites of phosphorylation detected by mass spectrometry are highlighted in yellow. (**D**) The presence of lamin-A,C fragments was also confirmed by MS in lower MW bands of A549 cell lysates. (**E**) MSCs were treated with a kinase-inhibitor (RO3306) and compared with non-treated control cells, with analysis performed by MS (with MW bands as shown in Fig. 3B). Changes in ion current of lamin-A,C peptides were assessed between samples. Enrichment of intermediate MW lamin fragments in RO3306-treated cells may be indicative of a phosphorylation event that is necessary for the progression of lamin cleavage.

(Related to Figs. 3F, G) Image analysis of cleaved lamin staining during inhibition of phosphorylation. (**F**) Representative images showing fixed MSCs, with and without kinase inhibitor RO3306 treatment, with immunostaining against lamin-A,C, pSer22 and cleaved lamin-A with either a monoclonal or a polyclonal antibody (data summarized in Figs. 3F, G). (**G**) Image analysis showed that lamin-A,C levels were ~50% higher and the projected area of the nucleus larger in drug-treated MSCs relative to non-treated cells, reminiscent of a highly contractile phenotype (n = 50-51 cells per group). (**H**) Cell-by-cell analysis of S22 phosphorylation in MSCs treated with kinase inhibitor RO3306 (Figs. 3F, G; S3F, G), plotted as a function of nuclear tension with hyperbolic-like fit consistent with the Mechanobiological Gene Circuit (MGC) model (Figs. 1F-H, 4E).

Figure S4.

A

Score	Molecular function	Celluar component	Biological process	Genes	
7.1	Cytoskeletal --> Actin filament binding	Cytoskeleton --> Actin	Actin filament bundle formation	LIMA1, EZR, ACTN4, FSCN1, ACTN1,…	DOWN
5.7	Cytoskeletal protein binding	Actin cytoskeleton, non-membrane-bound organell		PPP4R2, LIMA1, TUBB2A, ARPC4,TPM2, …	
4.7		Focal adhesion, cell junction		LIMA1, SYT11, NEXN, PERP, TES, VCL,…	
3.6		Cell cortex --> Cortical cytoskeleton		ACTB, EZR, ACTN4, LASP1, MYH9, DSTN,…	
3.4	Calponin-like actin-binding		Actin filament cytoskeleton organization	TAGLN, CNN2, CNN1,…	
2.8	Actin-binding	Calponin-like actin-binding		ACTN4, ACTN1, FLNA,…	
2.6	Microtubule cytoskeleton, centrosome			PPP4R2, NEDD1, KRT18, NDEL1, CALM3,…	
2		Muscle myofibril, sarcomere		ANK2, ACTN1, TPM2,…	
1.8	Leukocyte transendothelial migration	Adherens junction	Negative regulation of cell motion	ACTB, ACTN4, ACTN1, VCL,…	
1.8	Regulation of actin cytoskeleton	Focal adhesion	Calcium binding	FLG, CALM3, ACTN1,…	
1			Regulation of kinase activity	SPRY2, TRIB2, DUSP6	UP
0.8			Response to hormone stimulus	PLA2G4A, MGP, GNG11	
0.7			Positive regulation of apoptosis	PLA2G4A, TP53INP1, PHLDA1	

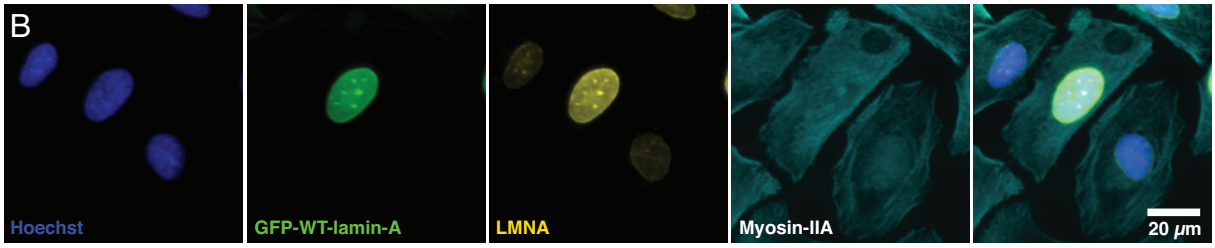

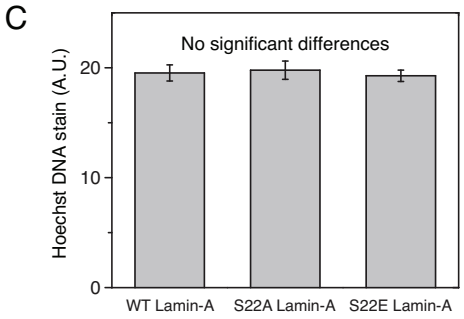

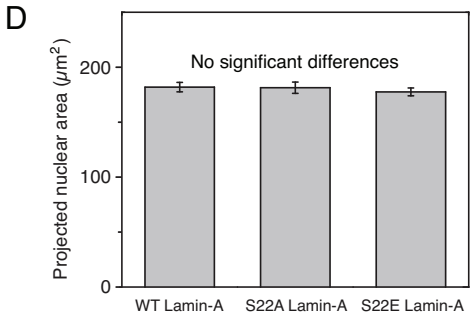

Figure S4.

(Related to Figs. 4A-C) GO-term analysis shows that lamin-A,C KD down-regulates actin cytoskeletal genes. (**A**) Gene ontology term analysis of the entire transcriptome shows that the cytoskeleton is broadly affected by lamin-A,C knockdown, consistent with perturbation to the serum response factor (SRF) pathway. The ten most significant changes, as evaluated by DAVID bioinformatics resources [S3], are instances of down-regulation, with seven of the ten (including the top three) related to the actomyosin cytoskeleton.

(Related to Figs. 4D, E) Lamin-A phosphomutations do not significantly affect chromatin or nuclear spreading in A549s. (**B**) Endogenous lamin-A,C was knocked down in A549 cells in conjunction with expression of GFP-lamin-A phosphomutant constructs (WT, S22A and S22E) in order to assess the effect on myosin-IIA. Representative images showed the expected localization of GFP-lamin-A at the nuclear envelope. Quantitative image analysis showed that neither Hoechst DNA staining (**C**) or nuclear spread area (**D**) were significantly altered by lamin-A phosphomutant expression (n = 70-113 cells per group).

Supplemental materials and methods

Isolation of fresh MSCs from bone marrow

Bone marrow aspirates were obtained from posterior iliac crest of anonymous human donors (University of Pennsylvania Stem Cell Core, with Institutional Review Board approval) under the procedures and regulations defined by the Helsinki agreement. Mono-nucleated cells (MNCs) were obtained using a Ficoll density gradient (Ficoll-Paque PLUS, GE Healthcare) and depleted from CD34-positive cells by a micro-bead kit (Direct CD34 Progenitor Cell Isolation Kit, Miltenyi Biotec) and screened by automated cell separation (AutoMacs, Miltenyi Biotec) according to manufacturer's protocols. MNCs were re-suspended in 10% FBS (Sigma-Aldrich) and 1% penicillin/streptomycin antibiotics (P/S, GE Healthcare) supplemented low-glucose basal medium (DMEM, Life Technologies). Typically, MNCs were seeded at 10-100k cells/cm² in standard tissue-culture plastic flasks and incubated at 37 °C and 5% CO2 humidified conditions. Cells were thoroughly rinsed in PBS x 3 after 24 hrs to remove non-adherent cells. Fibroblastic colony forming unit (CFU) stromal cells appeared within 3-4 days and cells expansion included medium exchange every 4 days. Cells confluence was maintained < 80% by passaging cells and re-seeding at > 50% confluence. Expression of stromal stem cells markers (CD105, CD166, CD44, CD90) and the lack of hematopoietic markers (CD45-RA, CD34) was verified by flow cytometry (data not shown). Differentiation capacity towards fat and bone was verified by adipogenic and osteogenic induction media (R&D: following manufacturer's protocols; data not shown). Fresh human CD34-positive cells were obtained by cell sorting from the mono-nucleated fraction of donor bone-marrow cells. Cells were cultured for seven days with stem cells factor (SCF) and thrombopoietin (TPO) for four days.

Preparation of soft and stiff hydrogel substrates

Adapted from [S4]. Glass cover slips (thickness #1.5, Fisher Scientific) were placed in boiling ethanol for 10 min, rinsed in distilled water (DW) and immersed in RCA (DW, hydrogen peroxidase (30%, Fisher Scientific), ammonium hydroxide (30%, Fisher Scientific) at 3:1:1 v/v) at 80 °C for 10 min and rinsed in DW. To remove water traces, glasses were rinsed in ethanol and then in chloroform and silanized in 0.1% allyltrichlorosilane (ATCS, Aldrich) in chloroform (Fisher Scientific) for 30 min. Silanized glasses were then

rinsed in chloroform, ethanol and DW and dried under vacuum. PA gel precursors were prepared by mixing acrylamide (AA, 40%, Sigma) and N,N'-methylenebisacrylamide (bis-AA 1.5% w/v in DW, Sigma) in PBS (Sigma). Gelation was initiated by adding 0.1% v/v tetramethylethylenediamine (TEMED, Sigma) and 0.1% w/v ammonium persulfate (Sigma) to gel precursor just before placing it at the center of the silanized cover slips and covering with RCA-treated glasses. Gels were allowed to polymerize while covalently binding the silanized glasses for 30-60 min. Non-silanized glasses were gently removed after immersing in PBS for 1-2 hours. Nominal gel elasticity was specified by varying acrylamide and cross-linker concentrations as calibrated by desktop rheometer. Gels were immersed in 10 mg/ml sulfo-SANPAH (Fisher Scientific) in 50 mM, pH 8.5 HEPES and reacted under 365 nm i-line exposure for 10 min. Collagen was mixed in 0.1 M acetic acid (Fisher Scientific) at equal volume and in 50mM, pH 8.5 HEPES to reach 0.2 mg/ml final concentration. Gels were immersed with collagen while agitated overnight at 37 °C. Prior to seeding cells, gels were UV-sterilized (cell culture hood UV light source) for three hours. During all preparation steps, gels were maintained in a hydrated state.

siRNA and shRNA knockdown of MYH9, LMNA; myosin-IIA and kinase inhibitors

All siRNAs used in this study were purchased from Dharmacon. Cells were passaged > 24 hours prior to transfection were and incubated with a complex of siRNA (30 nM; siLMNA: 5'-GGUGGUGACGAUCUGGGCU-3'; siMYH9: 5'-GGCCAAACCUGCCGAAUAAAUU-3' with complement sequence 5'-UUUAUUCGGCAGGUUUGGCCUU-3' or scrambled siRNA siGENOME non-targeting siRNA #1 (Thermo Fisher Scientific)) and 1 μg/mL Lipofectamine 2000 according to the manufacturer's instructions for 24 hours (in low glucose DMEM with 10% FBS). shLMNA construct (Sigma, TRCN0000061833: 5'-CGACTGGTGGAGATTGACAAT-3') was packed into a lentiviral delivery system, transduced into A549s by 1 μg/mL Polybrene for 72 hours and selected with 2 μg/mL puromycin. Racemic blebbistatin (EMD) was used at 30 μM (24 hr treatment). Kinase inhibitor RO3306 (Adipogen International) was used at 3.5 μM for no longer than 6 hours.

Transfection and transductions of lamin-A, myosin-IIA and respective phosphomimetic constructs

For MSCs: a construct expressing GFP-lamin-A under the EF1-alpha promoter [S5] was packed into a lentiviral delivery system. Cells were transduced at MOI 50 and evaluated for survival and proliferation (data not shown). The fraction of GFP-lamin-A positive cells prior to experiment was ~ 50%. GFP-positive cells were seeded on 6-well plates at very low density (less than one cell per 4X objective field of view). Colonies of GFP-lamin-A expressing MSCs were isolated using a cloning cylinder (Bel-Art Products, Pequannock, NJ), trypsinized and further expanded for experiments. Lamin-A constructs were transfected via electroporation following manufacturer's protocols (MSCs kit, Nucleofector; Lonza); myosin-IIA constructs were transfected using Lipofectamine LTX with Plus reagent (Invitrogen), using 0.5 g DNA per well of a 6-well plate. For A549s: Transfections were performed with Lipofectamine LTX/Plus reagent (Invitrogen), as above. Transfection levels were similar across all constructs (within 20-30%) based on GFP intensities and densitometry of immunoblots (not shown). Phosphomutant constructs were packed into a lentiviral delivery system and transduced into lamin-A knockdown A549s. Transduction efficiencies ranged from 60-90%.

Plasmid constructs for WT GFP-myosin-IIA were obtained from Addgene. GFP-lamin-A and S1943D GFP-myosin-IIA plasmids were generous gifts from C. H. June (University of Pennsylvania, PA), D. M. Gilbert (State University of New York, Syracuse) and A. Bresnick (Albert Einstein College of Medicine, Bronx, NY). GFP-Lamin-A S22A, S22D and S22E plasmids were constructed by standard site directed mutagenesis (Stratagene).

Immunofluorescence imaging

Cells were fixed with 3.7% formaldehyde (Sigma-Aldrich) in PBS for 10 min at RT followed by PBS washing 2X for 5 min. Blocking and primary antibody staining was performed in 1% BSA in PBS. Primary antibody concentrations ranged between 1/300 – 1/500, depending on the stock concentration, and all primary antibodies were incubated at RT for 2 h or overnight at 4°C. All donkey secondary antibodies (Alexa Fluor dyes 488, 564, and 647) were stained for 1-2 hours at RT at 1:500 dilution in PBS and

TRITC-phalloidin (Sigma-Aldrich) was used at a concentration of 100 ng/ml. Imaging for quantitative immunofluorescence of lamin-A, myosin-IIA and related phosphorylation-specific antibodies was performed using an inverted microscope (IX-71; Olympus) with either 20X (Olympus, NA-0.75) or 40X (NA-0.60) objectives, and a cooled CCD camera (Cascade; Photometrics) and image acquisition performed with Image Pro software (Media Cybernetics). Fixed cells were immuno- and histochemically-stained using the following antibodies and reagents: Myosin-IIA (mouse), monoclonal HSP90AB1 (Abcam); lamin-A,C pSer22, monoclonal cleaved lamin-A,C (Cell Signaling); polyclonal myosin-IIA, monoclonal lamin-A,C (mouse), polyclonal lamin-A,C (goat), polyclonal lamin-B1,2 (mouse), polyclonal cleaved lamin-A,C (Santa Cruz); polyclonal myosin-IIA, Phalloidin (Sigma). Fixed cells were mounted in mounting medium (Axell). To prevent volume distortions, samples prepared for confocal z-stacks quantification were not mounted. Prior to each experiment, lamp intensity and field of view homogeneity were calibrated pixel by pixel, relative to a fluorescent plastic standard. Image analysis was performed with in-house MatLab code that included background subtraction, cell and nuclear registration and intensity integration, morphological and statistical analyses.

Confocal microscopy

Laser scanning confocal fluorescence microcopy was carried out using the following systems: Leica Microsystems TCS SP8, 63×/ NA1.4 oil immersion objective (Fig. 2C) and Olympus Fluoview FV1000, 150X/NA1.45 or 60X/NA1.2 oil immersion objectives (Fig. 1A). Nuclear cross-sections orthogonal to the substrate were generated from 0.21 μm Z-stacks and constructed using Fiji [S6].

Fluorescence recovery after photobleaching (FRAP)

Confocal time-lapse imaging was acquired at 37 °C with 5% CO_2 in a humidified chamber with an inverted spinning-disk microscope (IX-81; Olympus) with a 14-bit high-resolution charge-coupled device (CCD) camera (HQ2; Photometrics) and MetaMorph software (Molecular Devices). Time lapse images were acquired with a 40X (Olympus, NA-0.75) and 60X water immersion lens (Olympus, NA-1.2), every 20 sec for 5-10 min after photobleaching. Cells were imaged in phenol-red free low glucose medium (DMEM, Life

Technologies) with 10% FBS and 1% penicillin/streptomycin. Image sequences were analyzed using MatLab custom designed code to quantify fluorescence recovery kinetics. After the first day cells were treated with 30 μM racemic blebbistatin (EMD; 24 hrs). Blebbistatin was washed out prior to FRAP in order to prevent light-induced toxicity.

Immunoblotting

Cells were trypsinized, pelleted and stored at -20 °C until analysis. Pellets were thawed and re-suspended in 1X LDS lysis buffer supplemented with 1% protease and 1% phosphatase inhibitors and sonicated on ice (3 x 15 x 1 s pulses, intermediate power setting). After resting for 30 min on ice, samples were denatured at 80 °C with 0.5% β-mercaptoethanol v/v for 10 min. Samples were loaded onto bis-Tris 4-12% gradient gels for electrophoresis (100 V x 10 min; 160 V x 55 min) and then transferred (iBlot; Life Technologies: settings P3, 7 min) to blotting membrane. Band intensities were quantified using Fiji/ImageJ, relative to local background levels flanking the specific bands.

Quantitative, label-free mass spectrometry

SDS-PAGE gels (NuPAGE 4-12% Bis-Tris, Invitrogen) were run at 100 V for 10 min and 160 V for 25 min. Gel sections were washed (50% 0.2 M ammonium bicarbonate (AB) solution, 50% acetonitrile (ACN), 30 min at 37 °C), dried by lyophilization, incubated with a reducing agent (20 mM tris(2-carboxyethyl)phosphine (TCEP) in 25 mM AB solution at pH 8.0, 15 min at 37 °C) and alkylated (40 mM iodoacetamide (IAM) in 25 mM AB solution at pH 8.0, 30 min at 37 °C). The gel sections were dried by lyophilization before in-gel trypsinization (20 μg/mL sequencing grade modified trypsin in buffer as described in the manufacturer's protocol (Promega), 18 hr at 37 °C with gentle shaking). The resulting solutions of tryptic peptides were acidified by addition of 50% digest dilution buffer (60 mM AM solution with 3% methanoic acid).

Peptide separations (5 μL injection volume) were performed on 15-cm PicoFrit column (75 μm inner diameter, New Objective) packed with Magic 5 μm C18 reversed-phase resin (Michrom

Bioresources) using a nanoflow high-pressure liquid chromatography system (Eksigent Technologies), which was coupled online to a hybrid LTQ-Orbitrap XL mass spectrometer (Thermo Fisher Scientific) via a nanoelectrospray ion source. Chromatography was performed with Solvent A (Milli-Q water with 0.1% formic acid) and Solvent B (acetonitrile with 0.1% formic acid). Peptides were eluted at 200 nL/min for 3–28% B over 42 min, 28–50% B over 26 min, 50–80% B over 5 min, 80% B for 4.5 min before returning to 3% B over 0.5 min. To minimize sample carryover, a fast blank gradient was run between each sample. The LTQ-Orbitrap XL was operated in the data-dependent mode to automatically switch between full scan MS (m/z = 350-2000 in the Orbitrap analyzer (with resolution of 60,000 at m/z 400) and the fragmentation of the six most intense ions by collision-induced dissociation in the ion trap mass analyzer.

Raw mass spectroscopy data was processed using Elucidator (version 3.3, Rosetta Biosoftware). The software was set up to align peaks in data from samples derived from corresponding molecular weight regions of the 1D gels. Peptide and protein annotations were made using SEQUEST (version 28, Thermo Fisher Scientific) with full tryptic digestion and up to 2 missed cleavage sites. Peptide masses were selected between 800 and 4500 amu with peptide mass tolerance of 1.1 amu and fragment ion mass tolerance of 1.0 amu. Peptides were searched against a database compiled from UniRef100 (November 2010) mouse, plus contaminants and a reverse decoy database. A deltaCn of 0.01 and mass error limit of 20 ppm was used, resulting in a false positive rate of ~10%. In these experiments, only proteins detected with three or more peptides were considered. The peptide database was modified to search for alkylated cysteine residues (monoisotopic mass change, Δ = +57.021 Da) and oxidized methionine (Δ = +15.995 Da). In proteomic profiling experiments, we also considered the acetylation of lysine (Δ = +42.011 Da), methylation of lysine and arginine (Δ = +14.016 Da), and phosphorylation of serine, tyrosine, threonine, histidine and aspartate (Δ = +79.966 Da). Ion currents of modified peptides were summed with their parent peptide. Peptides derived from trypsin or keratin were considered to be contaminants and were not used in subsequent calculations. When evaluating total ion current, only signals from annotated peptides were summed. The Peptide Ratio Fingerprinting algorithm was coded for Mathematica (version 8, Wolfram Research) and was used for all MS protein quantitation [S7].

Transcriptional profiling by DNA microarrays

Total RNA was extracted from cells using Trizol and purified by RNeasy (Qiagen) with on-column DNase digestion according to manufacturer's protocol. Adherent cells were gently scraped in Trizol. Total RNA was amplified and converted to cDNA using WT-Ovation Pico kit (NuGen). Fragmented and biotin-labeled ST-cDNA was generated using WT-Ovation Exon Module (NuGen). Samples were tested with Human Gene 1.0 ST DNA microarrays (Affymetrix), used according to the manufacturer's instructions. Expression data sets were analyzed by standard Robust Multi-array Averaging (RMA) methods.

Micropipette aspiration

Mesenchymal stem cells were harvested from culture, suspended in PBS + 1% BSA and treated in suspension with 0.5 μg/mL Latrunculin-A at 37 °C for 30 min. Cells were then washed with 1% BSA and re-suspended in 1% BSA supplemented with 0.2 μg/mL Latrunculin-A. A pulled glass micropipette was attached to a dual-stage water manometer with reservoirs of adjustable height. Suction was applied by syringe, and the corresponding pressure was measured by a pressure transducer (Validyne) calibrated with a mercury U-tube manometer. Pressures for different experiments were < 10 kPa. Images were acquired using a Nikon Eclipse TE300 inverted microscope using a 60X objective (Nikon, Plan Apo NA1.4) and a Cascade CCD camera (Roper Scientific). Images were captured every 30 sec over 5 min of aspiration at constant. Image were analyzed with ImageJ (NIH). Elastic stiffness was calculated according to previous work [S8]. Specifically, creep compliance $J(L) = \frac{2\pi}{3} \cdot \frac{2.1 \cdot L}{R \cdot \Delta P}$ was computed per each nucleus as a function of nuclear extension L at each time point and then fitted by $J(t) = A \cdot t^{\alpha}$. Nuclear relaxation times were computed with a threshold creep compliance overlapping with the dynamic range across conditions.

Systems Mechanobiology Gene Circuit (MGC) for coupled expression of lamin-A,C and myosin-IIA

Lamin-A,C (*L*) and myosin-IIA (*M*) message and protein circuitry is schematically presented in Figure 4F. In particular, expression kinetics of both are described by coupled rate equations for the respective transcripts (lower case) and proteins (upper case):

$$\frac{dl}{dt} = \alpha_1 \cdot L - \beta_1 \cdot l \quad \text{Eq. 1}$$

$$\frac{dL}{dt} = \gamma_1 \cdot l - \delta_1 \cdot \left(\frac{L^{n_L}}{K_L{}^{n_L} + L^{n_L}}\right) \quad \text{Eq. 2}$$

$$\frac{dm}{dt} = \alpha_2 \cdot M + \alpha_3 \cdot L - \beta_2 \cdot m \quad \text{Eq. 3}$$

$$\frac{dM}{dt} = \gamma_2 \cdot m - \delta_2 \cdot \left(\frac{M^{n_M}}{K_M{}^{n_M} + M^{n_M}}\right) \quad \text{Eq. 4}$$

For simplicity, RNA degradation and translation are assumed linear in transcript concentration. Lamin-A,C protein positively regulates one of its transcription factors, retinoic acid receptor (RAR), and myosin-IIA protein positively regulates one of its transcription factors, SRF, so that each enhances its own transcription (with rate constants α_1, α_2). In addition, lamin-A,C protein also enhances myosin-IIA transcription via the SRF pathway (rate constant α_3). Our results indicate a mechanical regulation of protein phosphorylation, and so we describe lamin-A,C and myosin-IIA protein turnover with suitable Hill models (rate constants δ_1, δ_2). Specifically, lamin-A,C protein turnover is suppressed by myosin-generated stress with $K_L = M^{n_K}$, while myosin-IIA protein turnover depends on matrix elasticity *E*: $K_M = \frac{E}{E+E_0}$.

A combined coordinate to describe nuclear tension and solutions to the MGC model

We sought to estimate a dimensionless measure of nuclear tension, σ, in terms of the stiffness of the nucleus, E_{nuc}, which depended on LMNA, and the nuclear strain, ε, which depended on changes in projected nuclear area, ΔA. In simplest form: $\sigma = E_{nuc} \cdot \varepsilon \sim \mathrm{LMNA}^m \cdot \Delta A^n$, where m = 2.5 conforms to scaling results for semi-flexible polymers [S9] as well as the enhanced nuclear viscosity with lamin-A,C [S10], and *n* = 0.5 is consistent with the scaling of strain with changes in nuclear radius (Fig. 1F). When pSer22/LMNA was plotted against this nuclear tension coordinate using data from analyses of immuno-fluorescence images (MSCs cultured on soft vs. vs. thin/soft vs. stiff substrate, Fig. 1C; MSCs subjected to lamin-A,C KD or blebb treatment, Figs 1E; S1F; MSCs treated with kinase inhibitor, Figs. 3F, G; S3F, G), the data collapsed well onto a hyperbolic-like decay consistent with the MGC model (Figs. 1G, H; S3H).

Equations 1-4 of the MGC model were solved numerically at steady state (all derivatives = 0) with free parameters adjusted to collectively obtain the best agreement with experimental data (fitting was performed using Mathematica, Wolfram). The rate of protein turnover was modeled as being proportional to tension *per molecule*. Cooperative protein turnover was $n_M = 10.4$ and $n_L = 2$ with the half-maximum effect on myosin-IIA turnover occurring at $E_0 = 5$ kPa. As matrix stiffness and cell tension suppressed protein phosphorylation and turnover, steady state levels monotonically increased with matrix *E*, consistent with coupled mechano-regulation of lamin-A and myosin-IIA. Maximal agreement was achieved with the model's free parameters set to the following values: $\alpha_1 = 4.43,\ \alpha_2 = 10, \alpha_3 = 2;\ \beta_1 = 1.4,\ \beta_2 = 1.5;\ \gamma_1 = 0.071,\ \gamma_2 = 2.3;\ \delta_1 = 3, \delta_2 = 10.9;\ n_K = 0.08, n_M = 10.4, n_L = 2$ (Fig. 4G).

Supplemental references

S1. Vicente-Manzanares, M., Ma, X.F., Adelstein, R.S., and Horwitz, A.R. (2009). Non-muscle myosin II takes centre stage in cell adhesion and migration. Nat. Rev. Mol. Cell Biol. *10*, 778-790.

S2. Raab, M., Swift, J., Dingal, P.C.D.P., Shah, P., Shin, J.-W., and Discher, D.E. (2012). Crawling from soft to stiff matrix polarizes the cytoskeleton and phosphoregulates myosin-II heavy chain. J. Cell Biol. *199*, 669-683.

S3. Huang, D.W., Sherman, B.T., and Lempicki, R.A. (2009). Systematic and integrative analysis of large gene lists using DAVID bioinformatics resources. Nat. Protoc. *4*, 44-57.

S4. Buxboim, A., Rajagopal, K., Brown, A.E.X., and Discher, D.E. (2010). How deeply cells feel: methods for thin gels. J. Phys.-Cond. Mat. *22*.

S5. Izumi, M., Vaughan, O.A., Hutchison, C.J., and Gilbert, D.M. (2000). Head and/or CaaX domain deletions of lamin proteins disrupt preformed lamin A and C but not lamin B structure in mammalian cells. Mol. Biol. Cell *11*, 4323-4337.

S6. Schindelin, J., Arganda-Carreras, I., Frise, E., Kaynig, V., Longair, M., Pietzsch, T., Preibisch, S., Rueden, C., Saalfeld, S., Schmid, B., et al. (2012). Fiji: an open-source platform for biological-image analysis. Nat. Methods *9*, 676-682.

S7. Swift, J., Harada, T., Buxboim, A., Shin, J.W., Tang, H.Y., Speicher, D.W., and Discher, D.E. (2013). Label-free mass spectrometry exploits dozens of detected peptides to quantify lamins in wildtype and knockdown cells. Nucleus *4*, 450-459.

S8. Dahl, K.N., Engler, A.J., Pajerowski, J.D., and Discher, D.E. (2005). Power-law rheology of isolated nuclei with deformation mapping of nuclear substructures. Biophys. J. *89*, 2855-2864.

S9. Gardel, M.L., Shin, J.H., MacKintosh, F.C., Mahadevan, L., Matsudaira, P., and Weitz, D.A. (2004). Elastic behavior of cross-linked and bundled actin networks. Science *304*, 1301-1305.

S10. Swift, J., Ivanovska, I.L., Buxboim, A., Harada, T., Dingal, P.C.D.P., Pinter, J., Pajerowski, J.D., Spinler, K.R., Shin, J.-W., Tewari, M., et al. (2013). Nuclear lamin-A scales with tissue stiffness and enhances matrix-directed differentiation. Science *341*, 1240104.